**Title:** *Pseudomonas aeruginosa* Siderophores Damage Lung Epithelial Cells and Promote Inflammation

**Authors:** Donghoon Kang, Natalia V. Kirienko

**Author Affiliations:** Department of BioSciences, Rice University, Houston, TX, USA

**Corresponding Author:** Natalia V. Kirienko; kirienko@rice.edu

**Abstract:**

Multidrug-resistant *Pseudomonas aeruginosa* is a common nosocomial respiratory pathogen that continues to threaten the lives of mechanically-ventilated patients in intensive care units and those with underlying comorbidities such as cystic fibrosis or chronic obstructive pulmonary disease. For over 20 years, studies have repeatedly demonstrated that the major siderophore pyoverdine is an important virulence factor for *P. aeruginosa* in invertebrate and mammalian hosts *in vivo*. Despite its physiological significance, an *in vitro,* mammalian cell culture model to characterize the impact and the molecular mechanism of pyoverdine during infection has only recently been developed. In this study, we adapt a previously-established murine macrophage-based model for human bronchial epithelial cells. We demonstrate that pyoverdine-rich conditioned medium from *P. aeruginosa* disrupts epithelial integrity in a manner that depends on protease activity and the type II secretion system. Disrupting pyoverdine production, whether genetically or chemically, mitigates this damage. Interestingly, this damage did not require exotoxin A or PrpL (protease IV), two previously-characterized toxins regulated by pyoverdine. We also examined the effects of exposure to purified pyoverdine on lung epithelial cells. While pyoverdine accumulates within cells, the siderophore is largely sequestered inside early endosomes, showing little cytotoxicity. This is in contrast to other, more membrane-permeable

iron chelators and siderophores such as pyochelin. However, pyoverdine may indirectly contribute to lung inflammation by potentiating these iron chelators in promoting the production of proinflammatory cytokines.

**Key Words:** *Pseudomonas aeruginosa*, Virulence, Siderophores, Lung Epithelial Cells, Protease, Neutrophilic Inflammation, Inflammasome

## Introduction:

Multidrug-resistant *Pseudomonas aeruginosa* is one of the most common respiratory pathogens infecting patients in intensive care units, especially those who are mechanically-ventilated or have chronic airway disorders like cystic fibrosis (CF) or chronic obstructive pulmonary disease (COPD) (Bhagirath et al., 2016; Hassett et al., 2014; Kollef et al., 2014; Lyczak et al., 2002; Murphy, 2009). This pathogen's intrinsic resistance to several classes of antibiotics and exceptional ability to form biofilms on medical devices and airway tissue pose a serious challenge for medical intervention (Anderson and O'Toole, 2008; Moreau-Marquis et al., 2008). In addition to colonizing the respiratory tract, *P. aeruginosa* actively deploys numerous virulence factors and toxins to damage host tissue, compromising pulmonary function (Curran et al., 2018). One of the major virulence factors produced by this pathogen is the siderophore pyoverdine.

Several groups have proposed possible mechanisms of pyoverdine-dependent virulence during lung infection. First and foremost, as a siderophore, pyoverdine scavenges ferric iron, providing a crucial nutritional need. Generally, iron acquisition serves an important function during *P. aeruginosa* infection by promoting bacterial growth and biofilm formation (Banin et al., 2005; Kang and Kirienko, 2018), and *P. aeruginosa* mutants lacking various iron uptake systems exhibit

attenuation of virulence during murine lung infection (Minandri et al., 2016). Pyoverdine-mediated iron uptake further promotes *P. aeruginosa* virulence by derepressing the alternative sigma factor PvdS, which activates the transcription of several virulence genes such as those encoding the translational inhibitor exotoxin A, exoprotease PrpL (protease IV), and pyoverdine biosynthetic enzymes (Lamont et al., 2002; Visca et al., 2007).

Of the two major siderophores secreted by *P. aeruginosa*, pyoverdine and pyochelin, pyoverdine is distinct in its ability to directly chelate iron from host ferroproteins such as transferrin and lactoferrin (Dumas et al., 2013; Xiao and Kisaalita, 1997). We have recently used a *Caenorhabditis elegans* nematode host model to demonstrate that pyoverdine may also directly chelate intracellular iron, disrupting mitochondrial homeostasis (Kang et al., 2018; Kirienko et al., 2015; Kirienko et al., 2013). Some combination of these various pathogenic functions makes pyoverdine production necessary for full *P. aeruginosa* virulence against murine hosts during acute lung infection (Imperi et al., 2013; Kang et al., 2019; Meyer et al., 1996; Minandri et al., 2016; Takase et al., 2000).

Recently, we established the first-reported *in vitro* cell culture model for pyoverdine-dependent virulence, where murine macrophages are treated with conditioned medium (also referred to as bacterial filtrate) from *P. aeruginosa* grown in serum-free cell culture medium (Kang and Kirienko, 2020). Under these conditions, *P. aeruginosa* exhibits robust pyoverdine production, yet the siderophore is not required for bacterial growth (**Figure 1A, B**), allowing pyoverdine's distinct role in virulence outside of its role in iron acquisition to be studied. This pyoverdine-rich conditioned medium from wild-type *P. aeruginosa* PAO1 is cytotoxic towards murine macrophages and murine alveolar macrophages (**Figure 1C)**, and in clinical isolates, pyoverdine content in conditioned medium positively correlates with cytotoxicity (Kang and Kirienko, 2020).

In this report, we adapt this *in vitro* pyoverdine virulence model for human bronchial epithelial cells to examine the consequences of pyoverdine production (i.e., pyoverdine and known pyoverdine-regulated virulence factors) during *P. aeruginosa* lung infection. We demonstrate that pyoverdine-rich conditioned medium from *P. aeruginosa* disrupts epithelial integrity in a protease-dependent manner. Genetic or chemical disruption of pyoverdine production mitigates this damage. Interestingly, this phenomenon depends on type II secretion but is independent of exotoxin A or PrpL production. We also examine the effects of purified pyoverdine exposure in lung epithelial cells. While pyoverdine accumulates within cells, the siderophore is largely sequestered within early endosomes and exhibits low cytotoxicity, in contrast to other more membrane-permeable iron chelators and siderophores such as pyochelin. However, we also demonstrate that pyoverdine may indirectly affect cell viability and promote neutrophilic inflammation in the presence of these chelators.

**Results:**

*Pyoverdine-rich conditioned medium disrupts epithelial integrity*

To investigate the role of pyoverdine production during *P. aeruginosa* lung infection, we treated human bronchial epithelial cells (16HBE) with pyoverdine-rich conditioned medium from *P. aeruginosa* PAO1 grown in serum-free cell growth medium (Eagle's Minimum Essential Medium). To visualize the integrity of the epithelial monolayer, we prelabeled cells with a plasma membrane stain. Within 1 h, the conditioned medium severely damaged the monolayer, causing more than half the cells to detach **(Figure 1D)**. This disruption was significantly attenuated in 16HBE cells treated with identically-prepared material from an isogenic pyoverdine biosynthetic mutant (PAO1*ΔpvdF*) but not a pyochelin mutant (PAO1*ΔpchBA*) **(Figure 1D, E)**. In the absence

of pyoverdine production, preventing pyochelin biosynthesis (*ΔpvdFΔpchBA*) did not confer further protection to 16HBE cells. One difference between these two siderophores is their affinity for ferric iron. Due to an exceptionally high affinity for the metal, pyoverdine is uniquely able to remove iron from host ferroproteins (Dumas et al., 2013; Xiao and Kisaalita, 1997). We examined whether host iron chelation was important for the damage we observed in the epithelial monolayer. To hinder pyoverdine's ability to bind iron, we pretreated the conditioned medium with a ferric iron mimetic, gallium ($Ga^{3+}$). However, even with the addition of excess gallium, there was no significant rescue **(Figure S1)**. Interestingly, we observed that removing large macromolecules greater than 10 kDa via centrifugal filtration or supplementing the conditioned medium with fetal bovine serum (FBS) abrogated the damage to the epithelial monolayer **(Figure S1)**. A common target for these two methods of intervention would be secreted *P. aeruginosa* proteases. Consistent with this hypothesis, supplementing the conditioned medium with a commercially-sourced protease inhibitor cocktail (capable of inhibiting serine and cysteine proteases) significantly lessened cell detachment **(Figure 1F, G, Figure S1)**.

*type II secretion is important for P. aeruginosa virulence against 16HBE cells*

Based on these results, we posited that the pyoverdine-regulated serine protease PrpL (protease IV) was primarily responsible for the damage we observed in 16HBE cells. To test this hypothesis, we prepared conditioned medium from an array of *P. aeruginosa* MPAO1 transposon mutants carrying insertions in *toxA* (exotoxin A), *prpL*, *xcpP*, or *xcpQ*, the latter two encoding proteins in the Xcp type II secretion system that is responsible for the secretion of exotoxin A and PrpL (Filloux, 2011). Due to a lack of a suitable wild-type strains, these transposon mutants were compared to those carrying mutations in antibiotic resistance genes (chloramphenicol

116 acetyltransferase *cat* and cephalosporinase *ampC*) that were irrelevant to our phenomenon of
117 interest. Conditioned medium from neither *toxA* nor *prpL* mutant resulted in significant attenuation
118 of cell detachment **(Figure 2A, B)**. However, we observed significant rescue in 16HBE cells
119 treated with conditioned medium from the two type II secretion mutants **(Figure 2A, B)**,
120 suggesting that this secretion system may transport additional pyoverdine-regulated proteases and
121 other toxins to damage epithelial cells.

122 To further demonstrate the importance of pyoverdine production in *P. aeruginosa* virulence
123 against lung epithelial cells, we took advantage of two clinical strains of *P. aeruginosa* isolated
124 from pediatric CF patients, PA2-9 and PA3-29. These two strains were selected from a collection
125 of CF isolates on the basis of their high *in vitro* pyoverdine production and virulence against the
126 nematode host *C. elegans* **(Figure S2)** (Kang et al., 2019). These two isolates were also amenable
127 to genetic manipulation, allowing us to generate mutants with transposon insertions in pyoverdine
128 biosynthetic enzymes **(Figure 2C, D, Table 1)**. As expected, 16HBE cells treated with conditioned
129 medium from wild-type PA2-9 exhibited severe disruption to the epithelial monolayer **(Figure**
130 **2E)**. This disruption was attenuated in the pyoverdine biosynthetic mutant (PA2-9 Tn) **(Figure 2E,**
131 **F)**. Importantly, we were also able to accomplish significant rescue by growing wild-type PA2-9
132 in the presence of the pyoverdine biosynthetic inhibitor 5-fluorocytosine (5-FC) at concentrations
133 where 5-FC does not affect bacterial growth **(Figure 2C, E, F)**. Notably, 5-FC has been
134 consistently shown to rescue various hosts from pyoverdine-dependent virulence (Costabile et al.,
135 2016; Imperi et al., 2013; Kang et al., 2019; Kang et al., 2021a; Kirienko et al., 2016).

136 In contrast, we did not observe any discernible damage to the epithelial monolayer by
137 conditioned medium from PA3-29, even though the strain exhibited comparable levels of
138 pyoverdine production and bacterial growth to that of PA2-9 **(Figure 2C-F)**. Whole genome

sequence analysis of PA3-29 revealed a 9 base-pair deletion in the Xcp type II secretion system gene XcpW. This is consistent with our observation that the type II secretion system is important for the disruption of epithelial integrity by *P. aeruginosa*.

*Pyoverdine translocates into 16HBE cells but is sequestered within early endosomes*

Next, we wanted to investigate the consequences of exposing 16HBE cells to pyoverdine in the absence of other virulence factors. In brief, pyoverdine-rich bacterial filtrate was subjected to two purification steps to separate small molecules by polarity: absorption and elution from a nonpolar polymeric resin (Amberlite XAD-4) and high-performance liquid chromatography (HPLC) via a C-18 reverse-phase column **(Figure S3)**. We tested whether this purified material was cytotoxic to 16HBE cells using a resazurin-based cell viability assay and compared its toxicity to other known iron-chelating molecules, including the ferric iron chelator ciclopirox olamine, the ferrous iron chelator 1, 10-phenanthroline, and deferoxamine, a siderophore produced by *Streptomyces spp*. While all other iron-chelators exhibited time- and dose-dependent cytotoxicity towards 16HBE cells, pyoverdine remained largely nontoxic even after 72 h treatment at 200 µM **(Figure 3A, Figure S4A, B)**.

Because pyoverdine is considerably larger than these iron-chelators, with a molecular weight of ~1365 g/mol, it may be unable to cross cellular membranes. We examined whether pyoverdine can translocate into 16HBE cells by taking advantage of its intrinsic spectral properties. After 24 h, 16HBE cells treated with purified pyoverdine accumulated pyoverdine **(Figure 3B, C)**. Consistent with previous studies, this intracellular fluorescence was enhanced when pyoverdine was pre-saturated with gallium and was quenched when pyoverdine was pre-saturated with iron **(Figure 3B, C)** (Kang et al., 2018; Kang and Kirienko, 2020). Importantly, pyoverdine

fluorescence did not colocalize with a plasma membrane stain, indicating that pyoverdine was primarily localized to the cytosol **(Figure S4C)**. However, we also observed that pyoverdine fluorescence formed distinct punctae within the cell. Based on previous observations in murine macrophages (Kang and Kirienko, 2020), we hypothesized that pyoverdine was sequestered within early endosomes. Supporting this hypothesis, pyoverdine colocalized with fluorophore-conjugated dextran, a well-established endosomal marker **(Figure 3D, Figure S4D)** (Oliver et al., 1984).

To investigate whether there was an endocytosis-independent route for pyoverdine internalization, we utilized giant plasma membrane vesicles (GPMVs) derived from 16HBE cells. We anticipated that these vesicles lacked the cellular machinery for complex molecular transport. Remarkably, these vesicles exhibited substantial accumulation of pyoverdine fluorescence following treatment. In contrast to the punctae observed in living cells, this fluorescence was evenly distributed throughout the vesicle **(Figure S5A-C)**. Pyoverdine within these vesicles remained fluorescent in the presence of excess ferric iron, unlike pyoverdine in solution **(Figure S5A)**. However, FITC-conjugated dextran showed a similar distribution as pyoverdine in GPMVs **(Figure S5D)**, suggesting that GPMVs may be more permeable to macromolecules than intact cells, as previously suggested by others (Skinkle et al., 2020; Zemljic Jokhadar et al., 2018). Altogether, while we were able to detect accumulation of intracellular pyoverdine in 16HBE cells, it appears to be sequestered within early endosomes, and it remains unclear whether pyoverdine can translocate across nonporous cellular membranes. These results are largely consistent with our observations that pyoverdine, unlike other iron-chelating molecules, exhibits low cytotoxicity towards 16HBE cells.

*Intracellular iron chelation activates an inflammatory response in 16HBE cells*

While pyochelin exhibits lower affinity towards ferric iron than pyoverdine, it is also substantially smaller, with a molecular weight of ~325 g/mol. We hypothesized that pyochelin may be able to enter 16HBE cells and chelate intracellular iron. While we were not able to visualize pyochelin internalization into cells (due to its lack of distinct spectral properties), one consequence of iron deprivation in epithelial cells would be a proinflammatory transcriptional response. Several studies have demonstrated that iron chelation by various siderophores such as deferoxamine and enterobactin promotes the production of proinflammatory cytokines, most notably interleukin (IL)-8 in lung epithelial cells, intestinal epithelial cells, and oral keratinocytes (Choi et al., 2004; Holden et al., 2014; Lee et al., 2007). To reaffirm these findings, we treated 16HBE cells with ciclopirox olamine (CPX), 1,10-phenanthroline (PHE), pyochelin (PCH), pyoverdine (PVD), or deferoxamine (DFO) and measured the mRNA levels of genes involved in neutrophilic inflammation. We first observed that total RNA yield (from phenol-chloroform extraction) in these cells corresponded with the resazurin-based cell viability assay **(Figure 3A, Figure S4A, B)**. Cells treated with cytotoxic iron chelators such as ciclopirox olamine, phenanthroline, and deferoxamine yielded substantially lower quantities of RNA, while cells treated with pyoverdine had quantities comparable to that of media control **(Figure 4A)**. Notably, RNA yield in cells treated with commercially-sourced pyochelin resembled that of ciclopirox olamine and phenanthroline. By qRT-PCR, we measured the expression of genes encoding components of the inflammasome, namely *NLRP3* and *NLRP1*, and those encoding the major proinflammatory cytokines produced by lung epithelial cells IL-1β (*IL1B*), IL-8 (*IL8*), and tumor necrosis factor alpha (*TNF*). Notably, all these genes have been associated with inflammation during lung infection (Moldoveanu et al., 2009). With the exception of pyoverdine, all iron chelators induced the expression of these proinflammatory genes **(Figure 4B)**. To ensure that this phenomenon was due to intracellular iron

chelation, we repeated the experiment with pyochelin and deferoxamine pre-saturated with excess gallium (1:2 stoichiometric ratio). Cells treated with gallium-bound pyochelin or deferoxamine exhibited RNA yields comparable to that of media control, suggesting that gallium inhibited the cytotoxic effects of the siderophores **(Figure 4C)**. Furthermore, pretreating the siderophores with gallium resulted in a significant decrease in proinflammatory gene expression **(Figure 4D)**, demonstrating that the chelator-induced inflammatory response was due to iron chelation rather than other nonspecific reactions or contaminants in the commercially-sourced material.

Finally, we investigated if pyoverdine can indirectly promote lung inflammation by potentiating other iron chelating molecules. Due to its exceptionally high affinity for iron, pyoverdine is likely to remove iron from other more cell-permeable siderophores or outcompete them for trace iron in the extracellular milieu, increasing the pool of apo-siderophores to disrupt host cell homeostasis and promote inflammation. To test this hypothesis, we treated 16HBE cells with deferoxamine, pyoverdine, or both. Cells treated with both siderophores exhibited greater cell death and increased expression of proinflammatory genes compared to those treated with deferoxamine alone **(Figure 4E, F)**. Considering that pyoverdine alone did not affect cell viability or transcription of proinflammatory genes, these results suggest that pyoverdine was able to potentiate deferoxamine-mediated damage by increasing the labile pool of apo-deferoxamine.

**Discussion:**

Arguably one of the greatest challenges to combating *P. aeruginosa* infections is the sheer multitude of virulence factors the bacterium can utilize to either directly or indirectly cause host damage. These include small molecule virulence factors (e.g., siderophores, quorum-sensing molecules), small molecule toxins (e.g., pyocyanin), factors involved in biofilm formation and

motility (e.g, exopolysaccharides, type IV pili, flagella), and more than twenty proteinaceous toxins that either directly kill host cells (e.g., exotoxin A, exoenzyme S, exotoxin T, exotoxin U) or damage host tissue (e.g., elastase LasA, elastase LasB, PrpL/protease IV, alkaline protease) (Hall et al., 2016; Hauser, 2009; Lee and Zhang, 2015; Michalska and Wolf, 2015; Thi et al., 2020). This complexity casts a dark shadow over the prospects of epidemiological or therapeutic intervention. In an ideal situation, we would be able to reliably predict a pathogen's ability to cause disease through our evolving molecular surveillance tools such as whole genome sequencing and mass spectrometry and therapeutically impair pathogenesis through anti-virulence drugs that inhibit the production or function of key virulence factors and toxins. In *P. aeruginosa*, the only feasible way to approach these strategies would be to unravel the regulation of virulence factors in the bacterium and to target virulence networks rather than individual factors.

The results we report in this study support the idea of targeting the alternative sigma factor PvdS, as has been investigated by others (Imperi reference). PvdS regulates the production of several secreted toxins such as the translational inhibitor exotoxin A and secreted protease PrpL. Exotoxin A, arguably one of the most extensively studied toxins in *P. aeruginosa*, inhibits protein synthesis (Michalska and Wolf, 2015), inducing airway epithelial cell death (Plotkowski et al., 2002) and potentially inhibiting cell junction repair in the presence of *P. aeruginosa* elastase (Azghani, 1996). Exotoxin A also contributes to *P. aeruginosa* virulence in various murine infection models (Hirakata et al., 1993; Miyazaki et al., 1995; Pillar and Hobden, 2002). Importantly, Ochsner and colleagues have demonstrated that *P. aeruginosa* exhibits a > 95% decrease in exotoxin A production in the absence of PvdS (Ochsner et al., 1996). PrpL contributes to the bacterium's overall extracellular proteolytic activity that is responsible for the responsible for the degradation of extracellular matrix and cell junction proteins and host defense proteins such

as surfactant proteins that contribute to innate immunity during *P. aeruginosa* lung infections (Malloy et al., 2005). Furthermore, PrpL has been shown to distinctly contribute to *P. aeruginosa* virulence during ocular infections (Engel et al., 1998; Engel et al., 1997) and degrade IL-22 to subvert lung epithelial immune response (Bradshaw et al., 2018; Guillon et al., 2017).

Of course, PvdS is best known for its role in pyoverdine biosynthesis and is indispensable for the production of pyoverdine biosynthetic enzymes. In addition to scavenging trace iron in the environment or directly from host ferroproteins, pyoverdine is involved in a positive feedback loop where the uptake of iron-bound pyoverdine by its outer membrane receptor derepresses PvdS by the inner membrane protein FpvR, increasing the production of pyoverdine, exotoxin A, and PrpL (Lamont et al., 2002; Visca et al., 2007). We have demonstrated here that pyoverdine production promotes the production of an additional secreted toxin, possibly a protease secreted by the type II secretion system, to damage the lung epithelium. Pyoverdine may also indirectly contribute to neutrophilic inflammation by removing iron from other more cell permeable siderophores such as pyochelin and enterobactin, the latter in the context of polymicrobial infections with *Enterobacteriaceae* such as the respiratory pathogen *K. pneumoniae* (Holden et al., 2016). Importantly, while *P. aeruginosa* may lose the ability to produce pyoverdine during lung infection with the emergence of social cheaters or due to a transition in iron acquisition strategy (Andersen et al., 2015; De Vos et al., 2001; Marvig et al., 2014), several surveys of patient sputum samples and clinical isolates have revealed that a large fraction of strains still exhibit substantial pyoverdine production (Haas et al., 1991; Kang et al., 2019; Martin et al., 2011; Mayer-Hamblett et al., 2014), demonstrating that pyoverdine may still represent an important target for therapeutic intervention.

Fortunately, the FDA-approved antimycotic drug, 5-fluorocytosine (5-FC) inhibits *pvdS* expression in *P. aeruginosa* and attenuates virulence during murine lung infection. Imperi and

277 colleagues first identified 5-FC in a screen for small molecules that inhibit pyoverdine production
278 (Imperi et al., 2013). We have independently identified a chemical analogue of 5-FC, 5-
279 fluorouracil – another inhibitor of *pvdS* inhibitor (Ueda et al., 2009), in a small molecule screen
280 for compounds that rescue *C. elegans* from *P. aeruginosa* in a pyoverdine-dependent pathogenesis
281 model (Kang et al., 2021b; Kirienko et al., 2016). We have also previously reported that 5-FC
282 synergizes with gallium nitrate, another FDA-approved drug, to inhibit *P. aerugino*sa growth and
283 virulence against *C. elegans* (Kang et al., 2021a). Our findings in this study suggest that in addition
284 to its bactericidal and biofilm-inhibitory activities (Goss et al., 2018; Kaneko et al., 2007), gallium
285 may also function as an anti-inflammatory agent during lung infection by inhibiting intracellular
286 iron chelation by pyochelin.

287 The benefits of suppressing neutrophilic inflammation during lung infection, particularly
288 chronic lung infection, has been well documented. While the mechanisms employed by neutrophils
289 to kill and remove pathogens, such as the production of neutrophil elastases, are important for host
290 defense, they also cause host tissue damage by degrading extracellular matrix proteins (Kruger et
291 al., 2015; Twigg et al., 2015). During chronic infections (such as those in CF patients), these host
292 defense factors continue to cause airway damage while the pathogen persists, exacerbating
293 pulmonary function decline (Cantin et al., 2015). While lung inflammation is mediated by many
294 factors in CF patients, a strategy to specifically inhibit the NLRP3 inflammasome by therapeutics
295 such as MCC950 is currently being investigated. This approach has shown promising results in
296 murine infection studies (Hosseinian et al., 2015; McElvaney et al., 2019). NLRP3 inflammasomes
297 have been shown to be activated by intracellular iron chelation in lung epithelial cells. We observed
298 this transcriptional response not only in wild-type 16HBE cells but also those carrying mutations
299 in the cystic fibrosis transmembrane conductance regulator (CFTR G551D, CFTR ΔF508), two of

the most frequently identified mutations in CF patients **(Figure S6)** (Estivill et al., 1997). Although gallium has been broadly associated with anti-inflammatory properties (Apseloff, 1999; de Albuquerque Wanderley Sales et al., 2021; Zhang et al., 2022), it has not been investigated for inhibiting pathogen-associated inflammation. Based on recent revelations that bacterial siderophores promote inflammation (Choi et al., 2004; Holden et al., 2016; Holden et al., 2014; Lee et al., 2007), this therapeutic avenue may merit consideration.

## Materials and Methods:

### *Bacterial Strains and Growth Conditions*

*P. aeruginosa* PAO1 and siderophore biosynthetic mutants were provided by Dr. Dieter Haas. The CF isolates PA2-9 and PA3-29 were provided by Dr. Carolyn Cannon (Kang et al., 2019). MPAO1 transposon mutants were from a commercially available library distributed by the University of Washington (Jacobs et al., 2003).

To produce pyoverdine-rich conditioned medium, a LB overnight culture of *P. aeruginosa* was diluted 20-fold into 2 mL of serum-free Eagle's Minimum Essential Medium in a 6-well plate. The plate was sealed with a Breath-Easy sealing membrane (Diversified Biotech, Dedham, MA) and grown statically at 37 ℃ for 16 h. Pyoverdine production (Ex. 405 nm; Em. 460 nm) and bacterial growth (OD 600nm) were measured spectrophotometrically. Bacteria was then removed by centrifugation and the supernatant was treated with an antibiotic cocktail to kill residual bacteria (100 µg/mL amikacin, 100 µg/mL gentamicin, 100 µg/mL tobramycin).

### *Cell Culture*

16HBE human bronchial epithelial cells were provided by Dr. Carolyn Cannon (Shah et al., 2020). 16HBE wild-type and CFTR mutant cell lines were provided by Dr. Gang Bao. All 16HBE cells were passaged in Eagle's Minimum Essential Medium (EMEM) (MilliporeSigma, Burlington, MA) supplemented with 10% fetal bovine serum, penicillin/streptomycin, and MEM non-essential amino acids.

For experiments with *P. aeruginosa* conditioned medium, $4\times10^6$ cells were seeded into each well of a collagen-coated 12-well plate and grown at 37 ℃ for 24 h in a $CO_2$-jacketed incubator by which they reached 100% confluence. To visualize the epithelial monolayer, cells were stained with 2.5 µg/mL CellMask Orange plasma membrane stain (Invitrogen, Carlsbad, CA) for 1 h prior to conditioned medium exposure. Following treatment, the medium was aspirated and the monolayer was imaged on a Cytation5 Multimode Reader (Biotek, Winnoski, VT) using a RFP filter cube. Percentage image area covered by fluorescent cells was quantified using ImageJ.

For cell viability measurements, 440µM resazurin (ThermoFisher Scientific, Waltham, MA) in phosphate buffered saline was diluted 10-fold into the treatment medium, and cells were incubated for 1.5 h. The medium was collected and briefly centrifuged to remove cells. 150 µL of the supernatant was transferred to a 96-well plate, and resorufin (reduced resazurin) fluorescence (Ex. 560 nm; Em. 590 nm) was measured on a Cytation5 Multimode Reader (Biotek, Winnoski, VT).

*Pyoverdine Purification*

A LB overnight culture of *P. aeruginosa* PAO1 was diluted 100-fold into 300 mL of M9 medium (1% w/v 5X M9 Salts (BD Difco, Franklin Lakes, NJ), 1.5% w/v Bacto Casamino Acids with low iron and salt content (BD Difco, Franklin Lakes, NJ), 1 mM $MgSO_4$, 1 mM $CaCl_2$) in a

345 2 L flask and grown aerobically for 24 h at 37 ℃. Bacteria was then removed by centrifugation
346 and filtration through a 0.22 µm membrane. The filtrate was incubated with 10% w/v amberlite
347 XAD-4 resin at RT for 4 h. After rinsing the resin with copious amounts of water, pyoverdine was
348 eluted in 50% methanol. This eluent was diluted in water to 15% MeOH and loaded onto a Luna
349 Omega 5 µm Polar C18 LC prep column (Phenomenex, Torrance, CA) for high-performance
350 liquid chromatography on a 1220 Infinity LC system (Agilent Technologies, Santa Clara, CA).
351 Pyoverdine was eluted from the column by a 0-100% methanol gradient across 4 h at a flowrate
352 of 5 mL/min. Fractions were collected every other minute for pyoverdine content analysis **(Figure**
353 **S3B)**. The fractions with the highest pyoverdine content were pooled. Methanol was removed from
354 this material using a SpeedVac vacuum concentrator. The final purified product was analyzed by
355 HPLC on an analytical column to verify sample purity **(Figure S3C)**.
356
357 *Confocal Laser Scanning Microscopy*
358 $8\times10^6$ 16HBE cells were seeded into each well of a collagen-coated 6-well plate and
359 grown at 37 ℃ for 24 h in a $CO_2$-jacketed incubator by which they reached 100% confluence.
360 After treatment, cells were washed in serum-free EMEM and detached from the microtiter plate
361 by trypsin-EDTA solution (MilliporeSigma, Burlington, MA). After inactivating the trypsin with
362 media containing 10% fetal bovine serum, the cells were concentrated via centrfiguation and
363 transferred onto a glass side with a 3% noble agar pad. These slides were visualized under a
364 LSM800 AiryScan confocal laser scanning microscope (Zeiss, Oberkochen, Germany).
365 Pyoverdine fluorescence was visualized via a 405 nm laser line using the channel conditions for
366 Pacific Blue. FITC-dextran fluorescence was visualized via a 488 nm laser line using channel
367 conditions for FITC. Dextran-Texas Red fluorescence was visualized via a 561 nm laser line using

368 channel conditions for Texas Red. CellMask Deep Red plasma membrane stain fluorescence was
369 visualized via a 640 nm laser line using channel conditions for Alex Fluor 660.

370 Giant plasma membrane vesicles from 16HBE cells were generated as previously described
371 (Gerstle et al., 2018). In brief, GPMV production was induced in a 100% confluent t-75 flask of
372 16HBE cells by a vesiculation buffer containing 1.9 mM DTT and 27.6 mM formaldehyde.
373 Pyoverdine or dextran treatment was directly applied to this GPMV/buffer. After treatment,
374 GPMVs were labeled with CellMask Deep Red plasma membrane stain then washed in
375 vesiculation buffer with centrifugation (16,000 g for 15 min) in between. GPMVs were transferred
376 onto a glass side with a 3% noble agar pad for confocal microscopy.

377

378 *qRT-PCR*

379 $8\times10^6$ 16HBE cells were seeded into each well of a collagen-coated 6-well plate and
380 grown at 37 ℃ for 24 h in a $CO_2$-jacketed incubator by which they reached 100% confluence.
381 After treatment, the medium was aspirated and cells were directly treated with TRI reagent
382 (Molecular Research Center, Cincinnati, OH) for phenol/chloroform/guanidinium thiocyanate
383 RNA extraction according to the manufacturer's protocols. Total RNA yield was quantified on a
384 Nanodrop spectrophotometer (ThermoFisher Scientific, Waltham, MA). cDNA synthesis was
385 performed on a Bio-RAD T100 Thermo Cycler (Bio-RAD, Hercules, CA) using a reverse
386 transcription kit (Applied Biosystems, Waltham, MA). qRT-PCR was performed on a Bio-RAD
387 CFX Connect Real-Time System (Bio-RAD, Hercules, CA) using a universal qPCR master mix
388 (New England Biolabs, Ipswich, MA). qPCR primer sequences are available upon request.

389

390 **Acknowledgements:**

This study was supported by funding from the Cystic Fibrosis Foundation (KIREIN20I0 to NVK; KANG19H0, KANG22H0 to DK), National Institutes of Health (R35GM129294 to NVK), and American Heart Association (903591 to DK). The authors declare no conflict of interest.

**Figure Legends:**

**Figure 1. Pyoverdine-rich conditioned medium causes lung epithelial cells to detach from the monolayer. (A, B)** Bacterial growth **(A)** and pyoverdine production **(B)** by *P. aeruginosa* PAO1 siderophore biosynthetic mutants (PAO1*ΔpvdF* – pyoverdine; PAO1*ΔpchBA* – pyochelin; PAO1*ΔpvdFΔpchBA* – pyoverdine and pyochelin) after 16 h growth in serum-free EMEM. **(C)** MH-S murine alveolar macrophage viability after 2 h exposure to conditioned media from PAO1 siderophore mutants grown in EMEM. **(D)** Fluorescent micrographs of 16HBE human bronchial epithelial cells after ~30 min exposure to conditioned media from PAO1 siderophore mutants grown in EMEM. Cells were prelabeled with CellMask Orange plasma membrane stain. **(E)** Quantification of percentage micrograph area covered by fluorescent cells. **(F, G)** Fluorescent micrographs of 16HBE cells after 30 min exposure to wild-type PAO1 conditioned medium pretreated with EDTA-free cOmplete Protease Inhibitor Cocktail or solvent control **(F)** and quantification of percent cell coverage **(G)**. Error bars in **A, B, C, E, G** represent SEM between four biological replicates. * corresponds to $p < 0.01$ and NS corresponds to $p > 0.05$ based on Student's *t* test.

**Figure 2. Damage to the epithelial monolayer is attenuated in conditioned medium from type II secretion-deficient strains. (A)** Fluorescent micrographs of 16HBE cells after 30 min exposure to conditioned media from MPAO1 transposon mutants grown in EMEM. Cells were prelabeled

with CellMask Orange plasma membrane stain. **(B)** Quantification of percentage micrograph area covered by fluorescent cells. **(C, D)** Bacterial growth **(C)** and pyoverdine production **(D)** by *P. aeruginosa* cystic fibrosis isolates PA2-9 and PA3-29, their pyoverdine biosynthetic mutant counterparts (Tn), and wild-type strain supplemented with 100 µM after 16 h growth in EMEM. **(E, F)** Fluorescent micrographs of 16HBE cells after 30 min exposure to conditioned media from *P. aeruginosa* cystic fibrosis isolates PA2-9 or PA3-29 **(E)** and quantification of percent cell coverage **(F)**. Error bars in **B, C, D, F** represent SEM between four biological replicates. * corresponds to $p < 0.01$ and NS corresponds to $p > 0.05$ based on Student's *t* test.

**Figure 3. Pyoverdine translocates into lung epithelial cells and localizes to early endosomes.** **(A)** 16HBE cell viability after 72 h treatment of ciclopirox olamine, 1, 10-phenanthroline, pyoverdine, or deferoxamine at 100 µM in serum-free EMEM. **(B)** Confocal micrographs of 16HBE cells exposed to 100 µM purified pyoverdine, pyoverdine with excess $Ga(NO_3)_3$, pyoverdine with excess $FeCl_3$, or media control for 24 h. Cells were trypsinated prior to imaging. **(C)** Quantification of pyoverdine fluorescence within 30 individual cells. **(D)** Confocal micrographs of 16HBE cells treated with 100 µM pyoverdine-gallium and dextran-Texas Red (10,000 MW). Error bars in **C** represent standard deviation. * corresponds to $p < 0.01$ based on Student's *t* test.

**Figure 4. Iron chelators promote the expression of proinflammatory genes in lung epithelial cells. (A)** Total RNA yield in 16HBE cells treated with ciclopirox olamine (CPX), 1,10-phenanthroline (PHE), or pyochelin (PCH) for 30 h and cells treated with pyoverdine (PVD) or deferoxamine (DFO) for 60 h normalized to that of media control. All treatments were at 100 µM

in serum-free EMEM. **(B)** Proinflammatory gene expression (*NLRP3, IL1B, NLRP1, IL8, TNF*) normalized to *ACTB* expression in 16HBE cells treated with iron chelators. mRNA levels were measured via qRT-PCR. **(C, D)** Total RNA yield **(C)** and proinflammatory gene expression **(D)** in 16HBE cells treated with iron chelators with or without excess $Ga(NO_3)_3$ supplementation. **(E, F)** 16HBE cell viability **(E)** and proinflammatory gene expression **(F)** after 60 h treatment with pyoverdine, deferoxamine, or both molecules. Error bars in **A-F** represent SEM between three biological replicates. * corresponds to $p < 0.01$, # corresponds to $p < 0.05$, and NS corresponds to $p > 0.05$ based on Student's *t* test.

**Supplementary Figure Legends:**

**Figure S1. Protease activity in pyoverdine-rich conditioned medium is important for the disruption of epithelial integrity. (A)** Fluorescent micrographs of 16HBE cells after ~30 min exposure to conditioned media from *P. aeruginosa* PAO1 grown in EMEM. Conditioned media were supplemented with 250 µM $Ga(NO_3)_3$, 5% fetal bovine serum (FBS), or EDTA-free cOmplete Protease Inhibitor Cocktail, or had macromolecules (> 10 kDa) removed by centrifugal filtration. Cells were prelabeled with CellMask Orange plasma membrane stain. **(B)** Quantification of percentage micrograph area covered by fluorescent cells. Error bars represent SEM between four biological replicates. * corresponds to $p < 0.01$ and NS corresponds to $p > 0.05$ based on Student's *t* test.

**Figure S2. PA2-9 and PA3-29 are highly virulent CF isolates. (A)** Pyoverdine production in M9 media by 69 multidrug-resistant *P. aeruginosa* strains isolated from pediatric cystic fibrosis patients. **(B)** Percent *C. elegans* death following Liquid Killing by *P. aeruginosa* cystic fibrosis

460 isolates. Black bar represents the median pyoverdine production/*C. elegans death*. Red bar
461 represents PA2-9, blue bar represents PA3-29. Survey data was adapted from (Kang et al., 2019).
462
463 **Figure S3. Purification of pyoverdine from *P. aeruginosa*. (A)** Summary of the pyoverdine
464 purification pipeline. **(B)** Representative chromatogram from the HPLC purification step of the
465 pipeline. Red box depicts the predominant pyoverdine-containing fractions that were collected. **(C)**
466 Analysis of the final purified product via HPLC.
467
468 **Figure S4. Pyoverdine accumulates in early endosomes of lung epithelial cells. (A, B)** 16HBE
469 human bronchial epithelial cell viability after 48 **(A)** or 72 h **(B)** treatment of ciclopirox olamine,
470 1, 10-phenanthroline, pyoverdine, or deferoxamine in serum-free EMEM. **(C)** Confocal
471 micrographs of 16HBE cells exposed to 100 µM purified pyoverdine, pyoverdine with excess
472 $Ga(NO_3)_3$, pyoverdine with excess $FeCl_3$, or media control for 24 h. Cells were labeled with
473 CellMask Deep Red plasma membrane stain and trypsinated prior to imaging. **(D)** Confocal
474 micrographs of 16HBE cells treated with 100 µM pyoverdine-gallium and dextran-Texas Red
475 (10,000 MW). Bottom row shows an enlarged micrograph of one representative cell.
476
477 **Figure S5. Pyoverdine translocates into giant plasma membrane vesicles. (A)** Pyoverdine
478 fluorescence quenching by $FeCl_3$ supplementation in GPMVs treated with 100 µM pyoverdine
479 (GPMV - PVD) or pyoverdine diluted in buffer control (Free PVD). **(B, C)** Confocal micrographs
480 of GPMVs **(B)** and 16HBE cells **(C)** treated with 100 µM pyoverdine or solvent control for 24 h.
481 GPMVs were labeled with CellMask Deep Red plasma membrane stain prior to imaging. 16HBE
482 cells were trypsinated prior to imaging. **(D, E)** Confocal micrographs of GPMVs **(B)** and 16HBE

cells **(C)** treated with FITC-dextran (3000 MW) or solvent control for 24 h. GPMVs were labeled with CellMask Deep Red plasma membrane stain prior to imaging. 16HBE cells were trypsinated prior to imaging.

**Figure S6. Deferoxamine promotes the expression of proinflammatory genes in 16HBE CFTR mutants. (A)** Total RNA yield in wild-type 16HBE cells and 16HBE cells carrying mutations (G551D, ΔF508) in the cystic fibrosis transmembrane conductance regulator (CFTR) after 48 h treatment with 100 µM deferoxamine in serum-free EMEM. **(B)** Proinflammatory gene expression (*NLRP3, IL1B, NLRP1, IL8, TNF*) normalized to *ACTB* expression in cells treated with deferoxamine. mRNA levels were measured via qRT-PCR. Error bars represent SEM between three biological replicates.

**References:**

Andersen, S.B., Marvig, R.L., Molin, S., Krogh Johansen, H., and Griffin, A.S. (2015). Long-term social dynamics drive loss of function in pathogenic bacteria. Proc Natl Acad Sci U S A *112*, 10756-10761.

Anderson, G.G., and O'Toole, G.A. (2008). Innate and induced resistance mechanisms of bacterial biofilms. Curr Top Microbiol Immunol *322*, 85-105.

Apseloff, G. (1999). Therapeutic uses of gallium nitrate: past, present, and future. Am J Ther *6*, 327-339.

Azghani, A.O. (1996). Pseudomonas aeruginosa and epithelial permeability: role of virulence factors elastase and exotoxin A. Am J Respir Cell Mol Biol *15*, 132-140.

505 Banin, E., Vasil, M.L., and Greenberg, E.P. (2005). Iron and Pseudomonas aeruginosa biofilm
506 formation. Proc Natl Acad Sci U S A *102*, 11076-11081.
507 Bhagirath, A.Y., Li, Y., Somayajula, D., Dadashi, M., Badr, S., and Duan, K. (2016). Cystic
508 fibrosis lung environment and Pseudomonas aeruginosa infection. BMC Pulm Med *16*, 174.
509 Bradshaw, J.L., Caballero, A.R., Bierdeman, M.A., Adams, K.V., Pipkins, H.R., Tang, A.,
510 O'Callaghan, R.J., and McDaniel, L.S. (2018). Pseudomonas aeruginosa Protease IV Exacerbates
511 Pneumococcal Pneumonia and Systemic Disease. mSphere *3*.
512 Cantin, A.M., Hartl, D., Konstan, M.W., and Chmiel, J.F. (2015). Inflammation in cystic fibrosis
513 lung disease: Pathogenesis and therapy. J Cyst Fibros *14*, 419-430.
514 Choi, E.Y., Kim, E.C., Oh, H.M., Kim, S., Lee, H.J., Cho, E.Y., Yoon, K.H., Kim, E.A., Han,
515 W.C., Choi, S.C., *et al.* (2004). Iron chelator triggers inflammatory signals in human intestinal
516 epithelial cells: involvement of p38 and extracellular signal-regulated kinase signaling pathways.
517 J Immunol *172*, 7069-7077.
518 Costabile, G., d'Angelo, I., d'Emmanuele di Villa Bianca, R., Mitidieri, E., Pompili, B., Del
519 Porto, P., Leoni, L., Visca, P., Miro, A., Quaglia, F., *et al.* (2016). Development of inhalable
520 hyaluronan/mannitol composite dry powders for flucytosine repositioning in local therapy of
521 lung infections. J Control Release *238*, 80-91.
522 Curran, C.S., Bolig, T., and Torabi-Parizi, P. (2018). Mechanisms and Targeted Therapies for
523 Pseudomonas aeruginosa Lung Infection. Am J Respir Crit Care Med *197*, 708-727.
524 de Albuquerque Wanderley Sales, V., Timoteo, T.R.R., da Silva, N.M., de Melo, C.G., Ferreira,
525 A.S., de Oliveira, M.V.G., de Oliveira Silva, E., Dos Santos Mendes, L.M., Rolim, L.A., and
526 Neto, P.J.R. (2021). A Systematic Review of the Anti-inflammatory Effects of Gallium
527 Compounds. Curr Med Chem *28*, 2062-2076.

528 De Vos, D., De Chial, M., Cochez, C., Jansen, S., Tummler, B., Meyer, J.M., and Cornelis, P.
529 (2001). Study of pyoverdine type and production by Pseudomonas aeruginosa isolated from
530 cystic fibrosis patients: prevalence of type II pyoverdine isolates and accumulation of
531 pyoverdine-negative mutations. Arch Microbiol *175*, 384-388.
532 Dumas, Z., Ross-Gillespie, A., and Kummerli, R. (2013). Switching between apparently
533 redundant iron-uptake mechanisms benefits bacteria in changeable environments. Proceedings
534 Biological sciences *280*, 20131055.
535 Engel, L.S., Hill, J.M., Moreau, J.M., Green, L.C., Hobden, J.A., and O'Callaghan, R.J. (1998).
536 Pseudomonas aeruginosa protease IV produces corneal damage and contributes to bacterial
537 virulence. Invest Ophthalmol Vis Sci *39*, 662-665.
538 Engel, L.S., Hobden, J.A., Moreau, J.M., Callegan, M.C., Hill, J.M., and O'Callaghan, R.J.
539 (1997). Pseudomonas deficient in protease IV has significantly reduced corneal virulence. Invest
540 Ophthalmol Vis Sci *38*, 1535-1542.
541 Estivill, X., Bancells, C., and Ramos, C. (1997). Geographic distribution and regional origin of
542 272 cystic fibrosis mutations in European populations. The Biomed CF Mutation Analysis
543 Consortium. Hum Mutat *10*, 135-154.
544 Filloux, A. (2011). Protein Secretion Systems in Pseudomonas aeruginosa: An Essay on
545 Diversity, Evolution, and Function. Front Microbiol *2*, 155.
546 Gerstle, Z., Desai, R., and Veatch, S.L. (2018). Giant Plasma Membrane Vesicles: An
547 Experimental Tool for Probing the Effects of Drugs and Other Conditions on Membrane Domain
548 Stability. Methods Enzymol *603*, 129-150.

549 Goss, C.H., Kaneko, Y., Khuu, L., Anderson, G.D., Ravishankar, S., Aitken, M.L., Lechtzin, N.,
550 Zhou, G., Czyz, D.M., McLean, K., *et al.* (2018). Gallium disrupts bacterial iron metabolism and
551 has therapeutic effects in mice and humans with lung infections. Sci Transl Med *10*.
552 Guillon, A., Brea, D., Morello, E., Tang, A., Jouan, Y., Ramphal, R., Korkmaz, B., Perez-Cruz,
553 M., Trottein, F., O'Callaghan, R.J., *et al.* (2017). Pseudomonas aeruginosa proteolytically alters
554 the interleukin 22-dependent lung mucosal defense. Virulence *8*, 810-820.
555 Haas, B., Murphy, E., and Castignetti, D. (1991). Siderophore synthesis by mucoid Pseudomonas
556 aeruginosa strains isolated from cystic fibrosis patients. Can J Microbiol *37*, 654-657.
557 Hall, S., McDermott, C., Anoopkumar-Dukie, S., McFarland, A.J., Forbes, A., Perkins, A.V.,
558 Davey, A.K., Chess-Williams, R., Kiefel, M.J., Arora, D., *et al.* (2016). Cellular Effects of
559 Pyocyanin, a Secreted Virulence Factor of Pseudomonas aeruginosa. Toxins (Basel) *8*.
560 Hassett, D.J., Borchers, M.T., and Panos, R.J. (2014). Chronic obstructive pulmonary disease
561 (COPD): evaluation from clinical, immunological and bacterial pathogenesis perspectives. J
562 Microbiol *52*, 211-226.
563 Hauser, A.R. (2009). The type III secretion system of Pseudomonas aeruginosa: infection by
564 injection. Nat Rev Microbiol *7*, 654-665.
565 Hirakata, Y., Furuya, N., Tateda, K., Kaku, M., and Yamaguchi, K. (1993). In vivo production of
566 exotoxin A and its role in endogenous Pseudomonas aeruginosa septicemia in mice. Infect
567 Immun *61*, 2468-2473.
568 Holden, V.I., Breen, P., Houle, S., Dozois, C.M., and Bachman, M.A. (2016). Klebsiella
569 pneumoniae Siderophores Induce Inflammation, Bacterial Dissemination, and HIF-1α
570 Stabilization during Pneumonia. MBio *7*.

571 Holden, V.I., Lenio, S., Kuick, R., Ramakrishnan, S.K., Shah, Y.M., and Bachman, M.A. (2014).
572 Bacterial siderophores that evade or overwhelm lipocalin 2 induce hypoxia inducible factor 1α
573 and proinflammatory cytokine secretion in cultured respiratory epithelial cells. Infect Immun *82*,
574 3826-3836.
575 Hosseinian, N., Cho, Y., Lockey, R.F., and Kolliputi, N. (2015). The role of the NLRP3
576 inflammasome in pulmonary diseases. Ther Adv Respir Dis *9*, 188-197.
577 Imperi, F., Massai, F., Facchini, M., Frangipani, E., Visaggio, D., Leoni, L., Bragonzi, A., and
578 Visca, P. (2013). Repurposing the antimycotic drug flucytosine for suppression of Pseudomonas
579 aeruginosa pathogenicity. Proc Natl Acad Sci U S A *110*, 7458-7463.
580 Jacobs, M.A., Alwood, A., Thaipisuttikul, I., Spencer, D., Haugen, E., Ernst, S., Will, O., Kaul,
581 R., Raymond, C., Levy, R., *et al.* (2003). Comprehensive transposon mutant library of
582 Pseudomonas aeruginosa. Proc Natl Acad Sci U S A *100*, 14339-14344.
583 Kaneko, Y., Thoendel, M., Olakanmi, O., Britigan, B.E., and Singh, P.K. (2007). The transition
584 metal gallium disrupts Pseudomonas aeruginosa iron metabolism and has antimicrobial and
585 antibiofilm activity. The Journal of Clinical Investigation *117*, 877-888.
586 Kang, D., Kirienko, D.R., Webster, P., Fisher, A.L., and Kirienko, N.V. (2018). Pyoverdine, a
587 siderophore from Pseudomonas aeruginosa, translocates into C. elegans, removes iron, and
588 activates a distinct host response. Virulence *9*, 804-817.
589 Kang, D., and Kirienko, N.V. (2018). Interdependence between iron acquisition and biofilm
590 formation in Pseudomonas aeruginosa. J Microbiol *56*, 449-457.
591 Kang, D., and Kirienko, N.V. (2020). An In Vitro Cell Culture Model for Pyoverdine-Mediated
592 Virulence. Pathogens *10*.

Kang, D., Revtovich, A.V., Chen, Q., Shah, K.N., Cannon, C.L., and Kirienko, N.V. (2019). Pyoverdine-Dependent Virulence of Pseudomonas aeruginosa Isolates From Cystic Fibrosis Patients. Front Microbiol *10*, 2048.

Kang, D., Revtovich, A.V., Deyanov, A.E., and Kirienko, N.V. (2021a). Pyoverdine Inhibitors and Gallium Nitrate Synergistically Affect Pseudomonas aeruginosa. mSphere, e0040121.

Kang, D., Zhang, L., and Kirienko, N.V. (2021b). High-Throughput Approaches for the Identification of Pseudomonas aeruginosa Antivirulents. mBio *12*.

Kirienko, D.R., Revtovich, A.V., and Kirienko, N.V. (2016). A High-Content, Phenotypic Screen Identifies Fluorouridine as an Inhibitor of Pyoverdine Biosynthesis and Pseudomonas aeruginosa Virulence. mSphere *1*.

Kirienko, N.V., Ausubel, F.M., and Ruvkun, G. (2015). Mitophagy confers resistance to siderophore-mediated killing by Pseudomonas aeruginosa. Proc Natl Acad Sci U S A *112*, 1821-1826.

Kirienko, N.V., Kirienko, D.R., Larkins-Ford, J., Wählby, C., Ruvkun, G., and Ausubel, F.M. (2013). Pseudomonas aeruginosa disrupts Caenorhabditis elegans iron homeostasis, causing a hypoxic response and death. Cell Host Microbe *13*, 406-416.

Kollef, M.H., Chastre, J., Fagon, J.Y., Francois, B., Niederman, M.S., Rello, J., Torres, A., Vincent, J.L., Wunderink, R.G., Go, K.W., *et al.* (2014). Global prospective epidemiologic and surveillance study of ventilator-associated pneumonia due to Pseudomonas aeruginosa. Crit Care Med *42*, 2178-2187.

Kruger, P., Saffarzadeh, M., Weber, A.N., Rieber, N., Radsak, M., von Bernuth, H., Benarafa, C., Roos, D., Skokowa, J., and Hartl, D. (2015). Neutrophils: Between host defence, immune modulation, and tissue injury. PLoS Pathog *11*, e1004651.

Lamont, I.L., Beare, P.A., Ochsner, U., Vasil, A.I., and Vasil, M.L. (2002). Siderophore-mediated signaling regulates virulence factor production in Pseudomonasaeruginosa. Proc Natl Acad Sci U S A *99*, 7072-7077.

Lee, H.J., Lee, J., Lee, S.K., Lee, S.K., and Kim, E.C. (2007). Differential regulation of iron chelator-induced IL-8 synthesis via MAP kinase and NF-kappaB in immortalized and malignant oral keratinocytes. BMC Cancer *7*, 176.

Lee, J., and Zhang, L. (2015). The hierarchy quorum sensing network in Pseudomonas aeruginosa. Protein Cell *6*, 26-41.

Lyczak, J.B., Cannon, C.L., and Pier, G.B. (2002). Lung infections associated with cystic fibrosis. Clin Microbiol Rev *15*, 194-222.

Malloy, J.L., Veldhuizen, R.A., Thibodeaux, B.A., O'Callaghan, R.J., and Wright, J.R. (2005). Pseudomonas aeruginosa protease IV degrades surfactant proteins and inhibits surfactant host defense and biophysical functions. Am J Physiol Lung Cell Mol Physiol *288*, L409-418.

Martin, L.W., Reid, D.W., Sharples, K.J., and Lamont, I.L. (2011). Pseudomonas siderophores in the sputum of patients with cystic fibrosis. Biometals *24*, 1059-1067.

Marvig, R.L., Damkiær, S., Khademi, S.M., Markussen, T.M., Molin, S., and Jelsbak, L. (2014). Within-host evolution of Pseudomonas aeruginosa reveals adaptation toward iron acquisition from hemoglobin. MBio *5*, e00966-00914.

Mayer-Hamblett, N., Rosenfeld, M., Gibson, R.L., Ramsey, B.W., Kulasekara, H.D., Retsch-Bogart, G.Z., Morgan, W., Wolter, D.J., Pope, C.E., Houston, L.S., *et al.* (2014). Pseudomonas aeruginosa in vitro phenotypes distinguish cystic fibrosis infection stages and outcomes. Am J Respir Crit Care Med *190*, 289-297.

McElvaney, O.J., Zaslona, Z., Becker-Flegler, K., Palsson-McDermott, E.M., Boland, F., Gunaratnam, C., Gulbins, E., O'Neill, L.A., Reeves, E.P., and McElvaney, N.G. (2019). Specific Inhibition of the NLRP3 Inflammasome as an Antiinflammatory Strategy in Cystic Fibrosis. Am J Respir Crit Care Med *200*, 1381-1391.

Meyer, J.M., Neely, A., Stintzi, A., Georges, C., and Holder, I.A. (1996). Pyoverdin is essential for virulence of Pseudomonas aeruginosa. Infect Immun *64*, 518-523.

Michalska, M., and Wolf, P. (2015). Pseudomonas Exotoxin A: optimized by evolution for effective killing. Front Microbiol *6*, 963.

Minandri, F., Imperi, F., Frangipani, E., Bonchi, C., Visaggio, D., Facchini, M., Pasquali, P., Bragonzi, A., and Visca, P. (2016). Role of Iron Uptake Systems in Pseudomonas aeruginosa Virulence and Airway Infection. Infect Immun *84*, 2324-2335.

Miyazaki, S., Matsumoto, T., Tateda, K., Ohno, A., and Yamaguchi, K. (1995). Role of exotoxin A in inducing severe Pseudomonas aeruginosa infections in mice. J Med Microbiol *43*, 169-175.

Moldoveanu, B., Otmishi, P., Jani, P., Walker, J., Sarmiento, X., Guardiola, J., Saad, M., and Yu, J. (2009). Inflammatory mechanisms in the lung. J Inflamm Res *2*, 1-11.

Moreau-Marquis, S., Stanton, B.A., and O'Toole, G.A. (2008). Pseudomonas aeruginosa biofilm formation in the cystic fibrosis airway. Pulm Pharmacol Ther *21*, 595-599.

Murphy, T.F. (2009). Pseudomonas aeruginosa in adults with chronic obstructive pulmonary disease. Curr Opin Pulm Med *15*, 138-142.

Ochsner, U.A., Johnson, Z., Lamont, I.L., Cunliffe, H.E., and Vasil, M.L. (1996). Exotoxin A production in Pseudomonas aeruginosa requires the iron-regulated pvdS gene encoding an alternative sigma factor. Mol Microbiol *21*, 1019-1028.

660 Oliver, J.M., Berlin, R.D., and Davis, B.H. (1984). Use of horseradish peroxidase and
661 fluorescent dextrans to study fluid pinocytosis in leukocytes. Methods Enzymol *108*, 336-347.
662 Pillar, C.M., and Hobden, J.A. (2002). Pseudomonas aeruginosa exotoxin A and keratitis in
663 mice. Invest Ophthalmol Vis Sci *43*, 1437-1444.
664 Plotkowski, M.C., Povoa, H.C., Zahm, J.M., Lizard, G., Pereira, G.M., Tournier, J.M., and
665 Puchelle, E. (2002). Early mitochondrial dysfunction, superoxide anion production, and DNA
666 degradation are associated with non-apoptotic death of human airway epithelial cells induced by
667 Pseudomonas aeruginosa exotoxin A. Am J Respir Cell Mol Biol *26*, 617-626.
668 Shah, K.N., Shah, P.N., Mullen, A.R., Chen, Q., Southerland, M.R., Chirra, B., DeBerardinis,
669 R.J., and Cannon, C.L. (2020). N-Acetyl cysteine abrogates silver-induced reactive oxygen
670 species in human cells without altering silver-based antimicrobial activity. Toxicol Lett *332*,
671 118-129.
672 Skinkle, A.D., Levental, K.R., and Levental, I. (2020). Cell-Derived Plasma Membrane Vesicles
673 Are Permeable to Hydrophilic Macromolecules. Biophys J *118*, 1292-1300.
674 Takase, H., Nitanai, H., Hoshino, K., and Otani, T. (2000). Impact of siderophore production on
675 Pseudomonas aeruginosa infections in immunosuppressed mice. Infect Immun *68*, 1834-1839.
676 Thi, M.T.T., Wibowo, D., and Rehm, B.H.A. (2020). Pseudomonas aeruginosa Biofilms. Int J
677 Mol Sci *21*.
678 Twigg, M.S., Brockbank, S., Lowry, P., FitzGerald, S.P., Taggart, C., and Weldon, S. (2015).
679 The Role of Serine Proteases and Antiproteases in the Cystic Fibrosis Lung. Mediators Inflamm
680 *2015*, 293053.

Ueda, A., Attila, C., Whiteley, M., and Wood, T.K. (2009). Uracil influences quorum sensing and biofilm formation in Pseudomonas aeruginosa and fluorouracil is an antagonist. Microb Biotechnol *2*, 62-74.

Visca, P., Imperi, F., and Lamont, I.L. (2007). Pyoverdine siderophores: from biogenesis to biosignificance. Trends Microbiol *15*, 22-30.

Xiao, R., and Kisaalita, W.S. (1997). Iron acquisition from transferrin and lactoferrin by Pseudomonas aeruginosa pyoverdin. Microbiology *143 ( Pt 7)*, 2509-2515.

Zemljic Jokhadar, S., Klancnik, U., Grundner, M., Svelc Kebe, T., Vrhovec Hartman, S., Liovic, M., and Derganc, J. (2018). GPMVs in variable physiological conditions: could they be used for therapy delivery? BMC Biophys *11*, 1.

Zhang, C., Yang, B., Biazik, J.M., Webster, R.F., Xie, W., Tang, J., Allioux, F.M., Abbasi, R., Mousavi, M., Goldys, E.M., *et al.* (2022). Gallium Nanodroplets are Anti-Inflammatory without Interfering with Iron Homeostasis. ACS Nano *16*, 8891-8903.

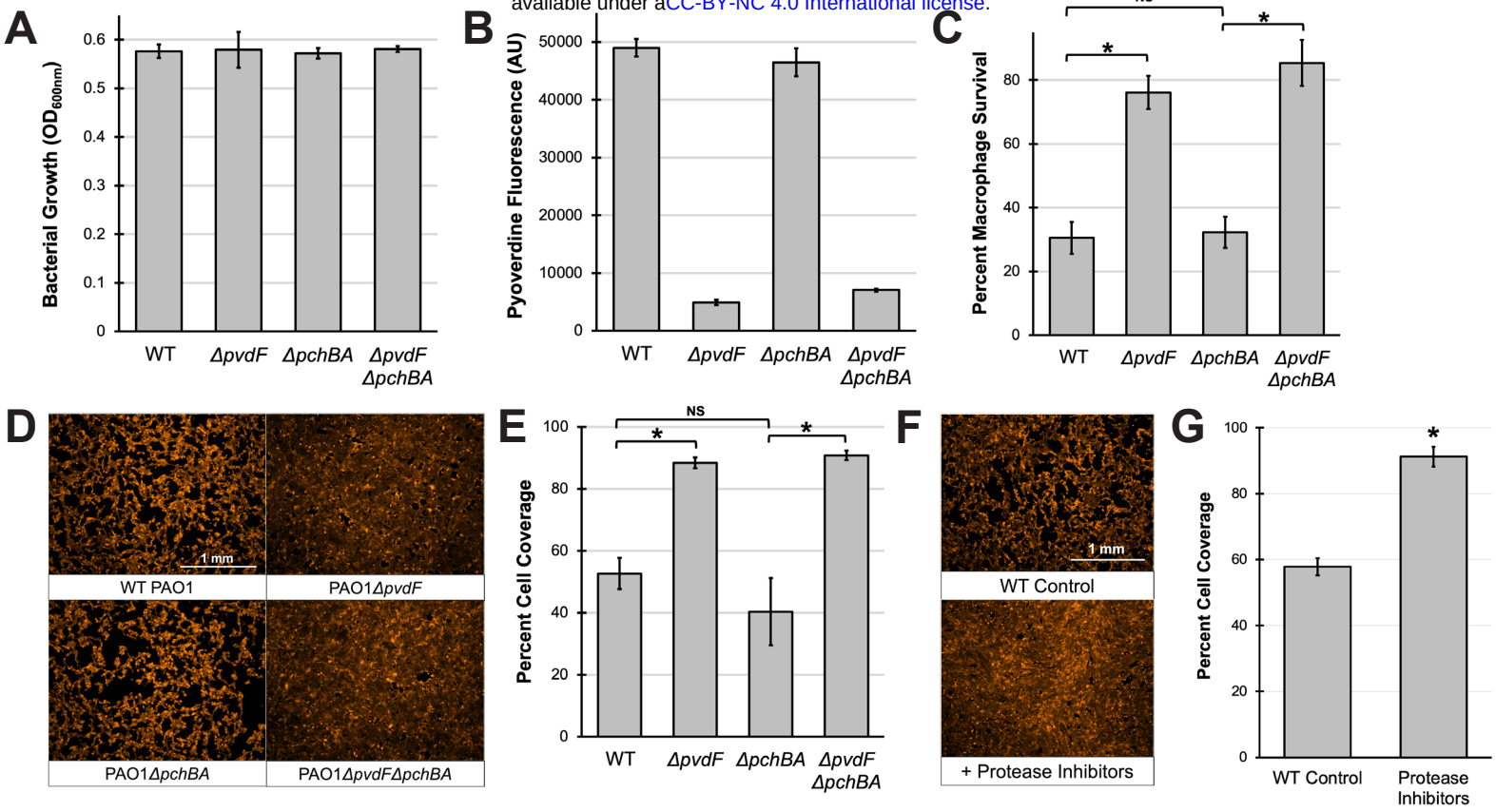


# Figure 1

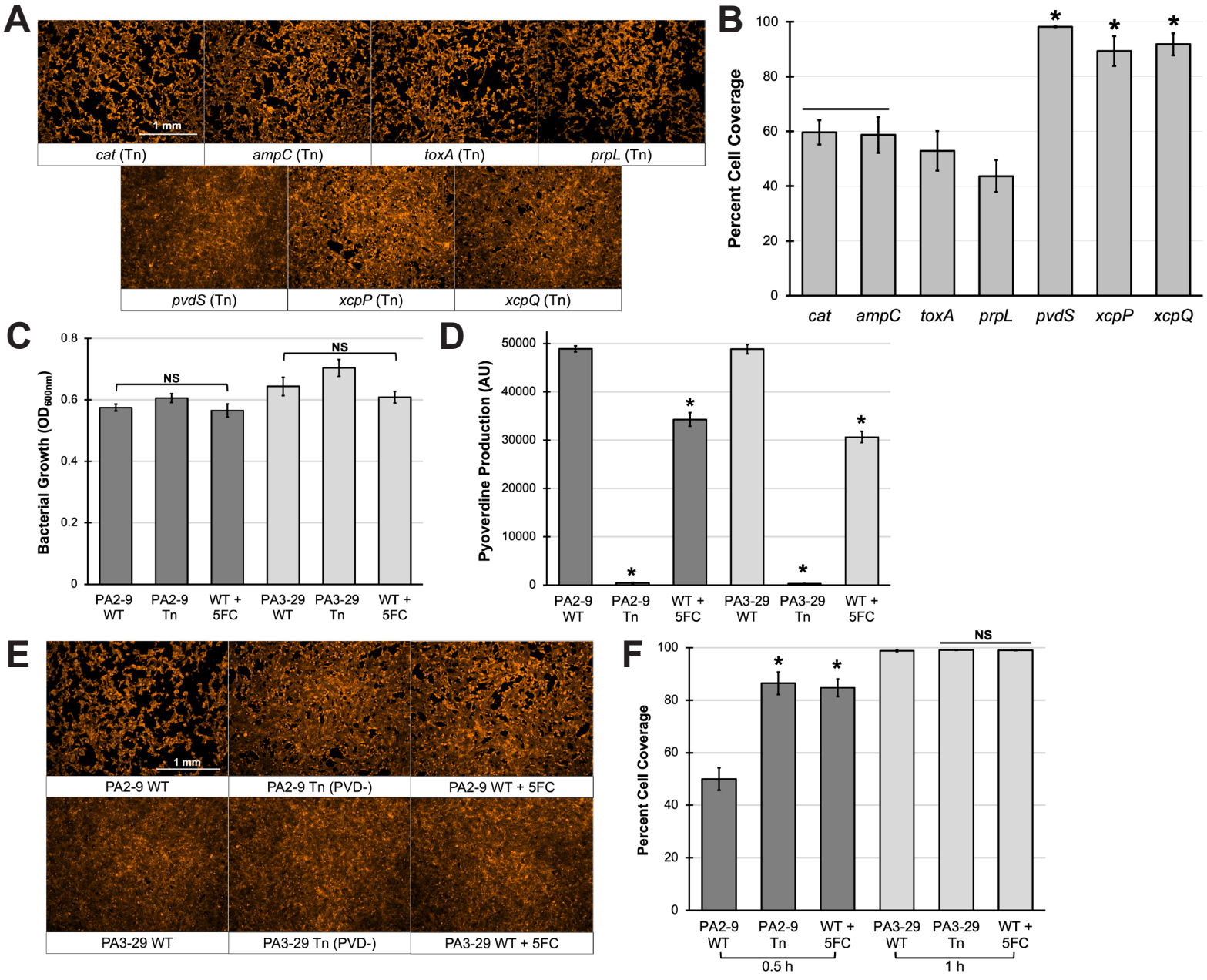


# Figure 2

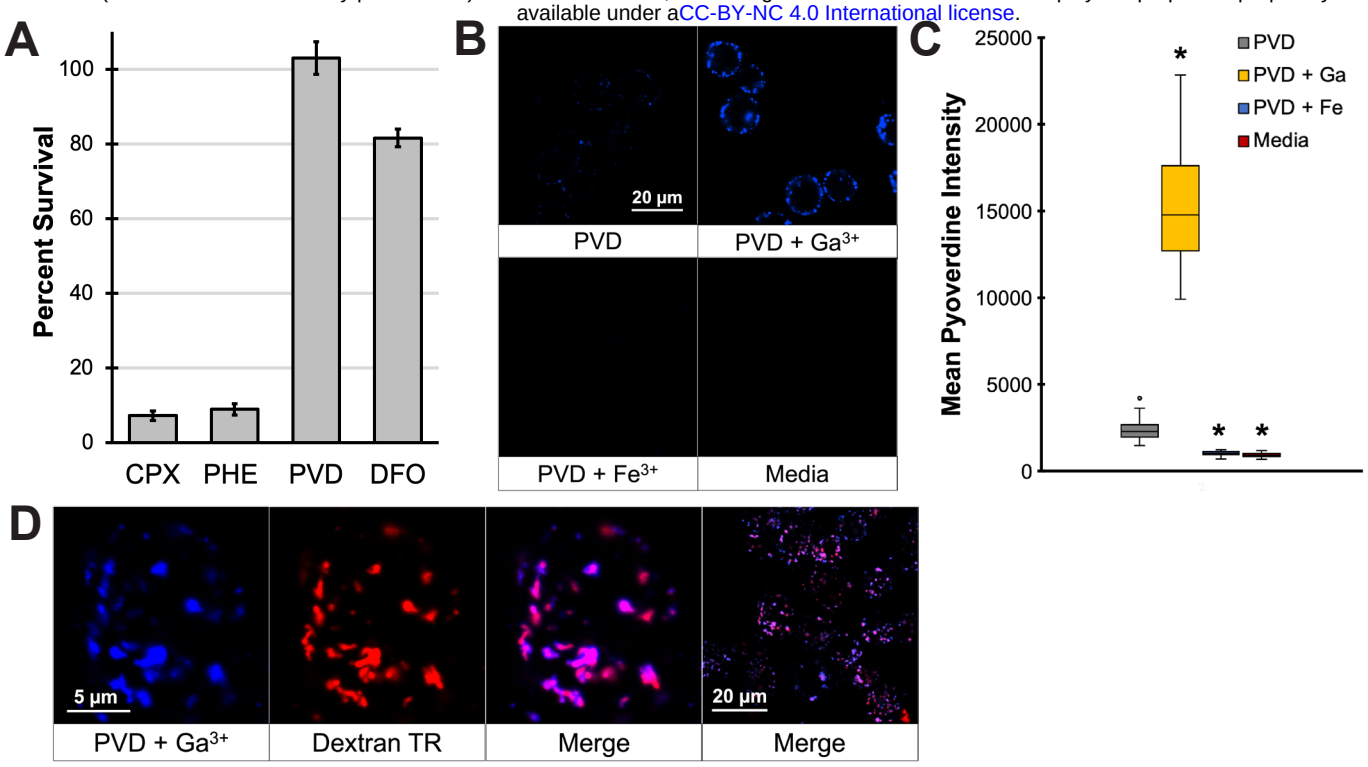


# Figure 3

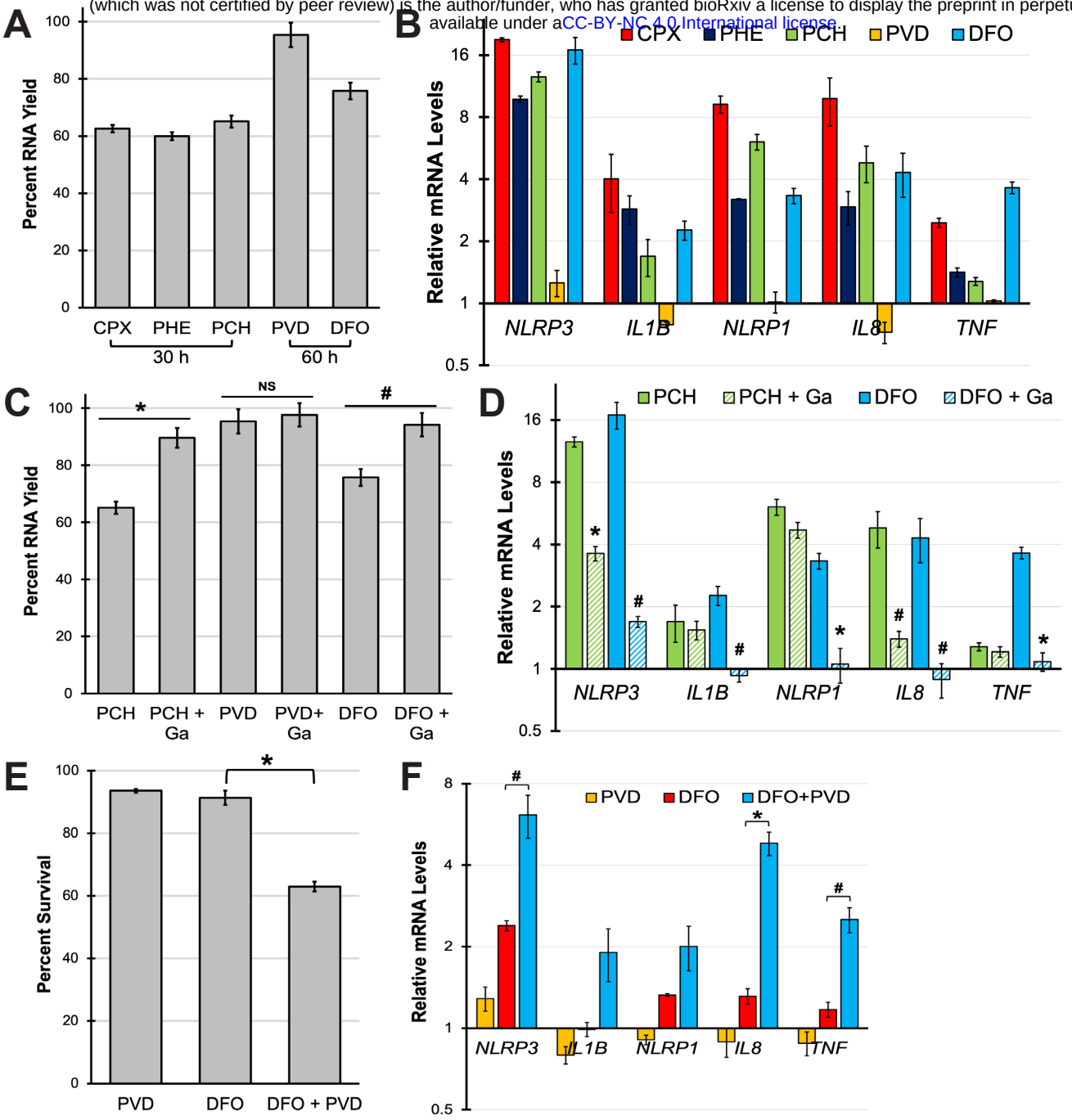


# Figure 4